Gold Nanorod Dimers as Nanoscale Optical Antennas

IISER PUNE

A thesis submitted towards partial fulfilment of
BS-MS Dual Degree Programme

by

Aswathy V. G.

under the guidance of

Dr. G. V. Pavan Kumar

Assistant Professor

INDIAN INSTITUTE OF SCIENCE EDUCATION AND RESEARCH
PUNE

Certificate

This is to certify that this thesis entitled **"Gold Nanorod Dimers as Nanoscale Optical Antennas"** submitted towards the partial fulfilment of the **BS-MS dual degree** programme at the **Indian Institute of Science Education and Research (IISER), Pune** represents original research carried out by **Aswathy V.G.** at IISER Pune, under the supervision of **Dr. G. V. Pavan Kumar** during the academic year **2014-2015**.

Aswathy V.G.
(Student)

Dr. G.V. Pavan
Kumar
(Supervisor)

Declaration

I hereby declare that the matter embodied in the report entitled **"Gold Nanorod Dimers as Nanoscale Optical Antennas"**are the results of the investigations carried out by me at the **Department of Physics, Indian Institute of Science Education and Research, Pune** under the supervision of **Dr. G.V. Pavan Kumar** and the same has not been submitted elsewhere for any other degree.

Aswathy V.G.
(Student)

Dr. G.V. Pavan Kumar
(Supervisor)

Publications

1. **Geometry-dependant anti-Stokes SERS radiation pattern from gold nanorod dimers**
   Aswathy V.G.,Partha Pratim Patra and G.V. Pavan Kumar
   (Manuscript under reveiw (2015))

2. **Directional out-coupling of light from a plasmonic nanowire-nanoparticle junction**
   Danveer Singh,Arindam Dasgupta,**Aswathy V.G.**,Ravi P.N. Tripathi and G.V. Pavan Kumar
   Opt. Lett. 40, 1006 (2015)

Dedicated to My Dearest Friend for whom a "Thank You" is just not enough...

Acknowledgements

Abstract

How to control and manipulate light at nanoscale by controlling the geometrical features of metallic nanostructures is the broad question we are trying to address in this thesis. The nanostructures we are interested in are single-crystalline gold nanorod monomers and dimers arranged in side-by-side coupled fashion, end-to-end connected manner and with specific inter-rod angles. Gold was chosen due to its biocompatibility as well as its spectral position in the visible region of the electromagnetic spectrum. Rod structure was considered due to its inherent anisotropy. We have synthesized gold nanorods of an average aspect ratio of 3 (60 nm length and 20 nm diameter) by a bottom-up method which results in single crystalline nanostructures and utilized UV-Vis absorption spectroscopy, field emission scanning electron microscopy (FE-SEM), transmission electron microscopy (TEM) and dark field optical microscopy for characterization. A commercial software 'Lumerical FDTD (finite-difference time domain) Solutions' was used to perform electro-dynamical simulations from which near-field and far-field characteristics were extracted for individual nanorods and dimers. The role of parameters like gap size, angle between dimers, excitation wavelength and polarization were investigated. Nanorod dimers at specific inter-rod angles exhibited asymmetric Fano-type spectral line profiles which resulted in anomalous near-field and far-field emission properties, when excitation wavelength hit the Fano-dip. Moreover, the far-field response was found to be very sensitive to the angle between nanorods, even though it did not appear so in the scattering spectra. In a nutshell, the potential of gold nanorod dimers as nanoscale optical antennas was demonstrated, which will have applications in designing directional light sources and Raman optical antennas.

Contents

Chapter 1

Introduction

The interaction between visible spectrum of electromagnetic radiation and matter is crucial to life. What could be more natural than mentioning the case of photosynthesis which utilizes sunlight, inorder to give an effective example for this? The perception that light cannot be focused down to a spot smaller than half of its wavelength persisted for a long time. This was mainly under the assumption that, there is a fundamental limit set by the wavelength of light (Abbe diffraction limit, $d = \lambda/2n\ Sin(\theta)$[1] where, λ is the wavelength of light, n is the refractive index of the surrounding medium and θ, the convergence angle (half of the angle subtended by the lens used for imaging)).

However, nanostructures make it achievable due to their inherent dimensional features. Among them, metallic nanostructures come to the forefront due to the presence of free electrons in them, which facilitate the confinement of ordinary light waves into extremely small spatial dimensions resulting in the concentration of huge amount of energy in small volumes. Essentially, optical components can be scaled down to dimensions comparable to that of even electrons and these nanostructures have the capability to focus light into spots those are about thousand times smaller than the ones made by any conventional lenses. These features find importance in a lot of applications in the field of nano-optics, electronics, sensing, biophysics etc. and hence demands thorough investigations on effective light-matter interactions at nanoscale using metallic nanostructures. The field of plasmonics deals with such studies. Among all the metals, gold and silver stands a step ahead due to their resonant behavior at optical wavelengths and their low loss factors relative to other metals. The spectral positions are also tunable by varying their geometrical features.

Anisotropic gold nanorods are the central theme of this work. Spectral and optical nanoantenna properties of gold nanorod monomers and dimers of different orientations were explored as a function of wavelength and polarization of light, as well as for interparticle separations.

1.1   Surface Plasmons

The optical properties of metals can be described by the plasma model, which consists of a sea of free electrons and a background of positive ion core.[2] When light is incident on a metallic structure, its electric field causes the electrons to move back and forth in the structure leaving a positive charge on the other side. Such oscillations of free electrons at the surface of a metal are called plasma oscillations. The collective oscillation (surface excitation) of electrons at a metal-dielectric interface, upon coupling with electromagnetic radiation is termed as a surface plasmon (SP), which can be considered as a quasiparticle. These fundamental excitations are of two types- surface plasmon polaritons (SPPs) and localized surface plasmons (LSPs). SPPs are the propagating, dispersive plasmon modes whereas LSPs are non-propagating and localized as the name itself indicates.[3] Here, we will focus on the properties of LSPs.

1.1.1   Localized surface plasmons

The origin of LSP modes is basically from the scattering scenario of a sub-wavelength metal nanoparticle in an oscillating electromagnetic field.[4] The effective restoring force exerted by the curved side of the particle on the electrons results in a resonance condition; plasmon modes get strongly localized at the surface and get discretized. One of the striking advantages of LSPs is that, they can be excited by direct light illumination which is not possible in the case of SPPs because of the greater value of their momentum vector (k) than that of a plane light wave.[2] Similar to the case where propagating waves are described by a wave vector, k, localized (standing) waves are described by the geometrical features of the structure.

A lot of theoretical descriptions have been developed to explain the interaction between electromagnetic field and small particles. In the quasistatic approximation where the particle size, d is much smaller than the wavelength of light ($d \ll \lambda$), the phase of the oscillating electromagnetic field can be considered as a constant inside the particle, which simplifies the problem to

that of a particle in an electrostatic field.[4] Here, a solution to the *Laplace's* equation,

$$\nabla^2 \phi = 0 \qquad (1.1)$$

where ϕ is the scalar potential gives the electric field as,

$$E = -\nabla \phi \qquad (1.2)$$

Such a simplification applies to nanoparticles of dimensions approximately below 100 nm. The extinction cross-section C_{ext} which is the sum of absorption and scattering cross-sections ($C_{ext} = C_{abs} + C_{sca}$) for the simplest geometry of a spherical nanoparticle calculated using quasi-static approximation is,

$$C_{ext} = 9\frac{\omega}{c}\epsilon_m^{3/2}V\frac{\epsilon_2}{[\epsilon_1 + 2\epsilon_m]^2 + \epsilon_2^2} \qquad (1.3)$$

Here, ϵ_m is the dielectric function of the medium and $\epsilon = \epsilon_1 + i\epsilon_2$ is the dielectric function of the sphere of volume V.

However, in the limit where quasi-static approximation fails, we have to take into account the significant phase changes of the electromagnetic field inside the nanostructure. In 1908, Gustav Mie has come up with a semi-analytical theory to determine the scattering and absorption of electromagnetic radiation by spheroidal or ellipsoidal particles of arbitrary refractive index.[5] The motivation was primarily to explain the colours of colloidal gold particles in solution.

Richard Gans in 1912 extended the theory for spheroidal particles[6]. For particles of arbitrary shape, no exact analytical solution exists and we have to seek numerical methods to model them and understand their optical properties.

1.2   Plasmonic nanorods

Plasmonic nanorods have attained a significant interest in the field of nanoplasmonics, mainly due to their inherent shape anisotropy. Unlike spherically symmetric nanostructures, nanorods having cylindrical symmetry support
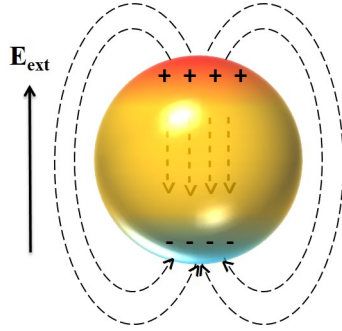
Figure 1.1: *Schematic of the dipolar plasmon mode of a spherical particle driven by an external electric field E_{ext}. The direction of field lines are shown.*
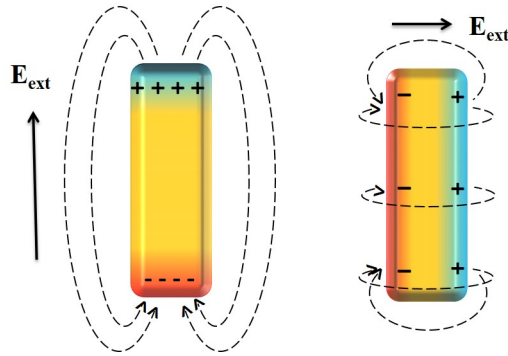
Figure 1.2: *Schematic of the smallest order longitudinal and transverse mode of a nanorod upon excitation with an electric field E_{ext}. The direction of E_{ext} and that of field lines are shown.*

two distinct kinds of plasmonic resonances - longitudinal and transverse, suggested by the Mie-Gans theory.[5] When an electric field drive charges along the long axis of the rod, longitudinal modes get excited and when it is perpendicular, transverse modes. The position of longitudinal mode is on the red side of the spectrum compared to the transverse one as electrons have to take a longer route in the former case. The schematic of dipolar plasmon mode from a spherical particle and its comparison with the two modes of nanorod is shown in the figure 1.1 and figure 1.2.

Both of these modes are dipolar and can be excited efficiently by plane waves. Though these structures can support higher order modes like quadrupolar and octupolar, exciting them is not straightforward as they have a zero net dipole moment and cannot be radiated into far-fields (non-radiative modes). Inorder to excite them, one has to use radiations having non-uniform elec-

tromagnetic fields.[7]

The resonant positions of longitudinal mode vary as a function of the aspect ratio of nanorod, but the effect is very less for the transverse mode. This tunability of longitudinal resonance is desirable for many practical applications. According to Gans theory, the position of longitudinal resonance is a function of nanorod aspect ratio and the permittivity of the medium, not on the absolute dimensions of the rod independently. From this theory, the longitudinal plasmon wavelength can be derived as,[7]

$$\lambda_{plasmon} = \lambda_p \sqrt{\epsilon_\infty + \left(\frac{1}{l} - 1\right)\epsilon_m} \tag{1.4}$$

$$\lambda_p = \sqrt{\frac{2\pi^2 c^2 m \epsilon_\infty}{Ne^2}} \tag{1.5}$$

Here, ϵ_∞ is the dielectric constant of gold, l is the depolarization factor along the long axis of the rod, m is the effective mass of electrons in gold, c is the speed of light, N is the density of conduction electrons and e is the charge of electrons.

However, recent studies have shown that even with a fixed aspect ratio, longitudinal resonance position can vary with a change in nanorod radius,[8] [9] which recommends further studies. It should also be noted that, since the size of the nanorod (radius and length) is much greater than the Fermi wavelength ($a \gg \lambda_F \sim 0.5$ nm), the classical description still holds and quantum effects can be neglected.

1.3   Nanorods as LC circuits

At the heart of circuital model of metallic structures lies the equivalent parametrization of the dielectric constant ϵ_m of a metal and the optical conductivity σ.[10] Starting from $Ampere's$ law, the impedance of a metallic wire can be calculated as,

$$Z = \frac{1}{\sigma(\omega)}\frac{length}{area} = \frac{1}{j\omega\epsilon_0(\epsilon_m - 1)} \times \frac{length}{area} \tag{1.6}$$

where j is the current and ω is the frequency.

When it comes to surface plasmons, the physics can be explained in terms of a distributive transmission line model, with slight modifications. The natural puzzle arises is that, how it is going to be possible with a single conductor, as the transmission model has two conductors - one to transmit the current and the second one to return the current. In the description of plasmonic nanostructures as circuits, the key lies in the fact that, the return currents essentially flow at infinity.[10]

Modelling a nanorod as an LC circuit having an inductance and capacitance is a new scheme to study its longitudinal plasmon resonance.[11] Illuminating the nanorod with light will be followed by a current flow I and a magnetic field whose amplitude is proportional to the current, would also be generated. This magnetic field energy, $LI^2/2$ will induce a self-inductance L. Since the magnetic energy which is inside the conductor is much smaller than that is outside, it is reasonable to consider only the latter. It has been shown that the energy is localized in a cylindrical region with length l, inner radius a and the outer radius $l/2$. The self-inductance can be calculated from the energy of this cylindrical region and it has a dominant contribution from the length of the nanorod.

$$L = \frac{\mu_0 l}{2\pi} ln\left(\frac{l}{2a}\right) \tag{1.7}$$

A formal inductance R_0 will also be produced as a result of the AC resistance offered by the nanorod, which can be calculated from the kinetic energy of electrons. This turns out to be inversely proportional to the cross-section which has a significant function in the nanocircuit.

The current flow in the rod causes the accumulation of electric charges with opposite signs on the opposite sides of the nanorod and hence each of the end faces act as a single circular capacitor. Here, the potential has a gradual decrease from the center to the edge faces. Taking into consideration the inhomogeneous nature of the potential and the weak coupling between two capacitors, the effective capacitance would be modified as,

$$C = \alpha\pi\epsilon_0\epsilon_d a \tag{1.8}$$

Here α is the correction coefficient, which can be calculated by comparing the analytical and numerical values of resonance positions. For gold nanorods

α has been found out to be 2.5. The important thing to note here is that, the effective capacitance of a nanorod is not governed by the aspect ratio or the absolute length, but indeed the radius and the permittivity of the surrounding medium.

1.4 Plasmonic molecules - Plasmon hybridization theory

Plasmon hybridization theory is the electromagnetic analogue of molecular orbital theory (MOT) which is developed by Peter Nordlander and co-workers in 2003[12]. This is an intuitive concept in which the plasmons of closely placed nanostructures interact, mix and then hybridize like electronic wave functions of atomic and molecular orbitals. New plasmonic states can be assigned as bonding or antibonding depending on the distribution of induced charges and hence such structures can be called as plasmonic molecules or artificial molecules.[13]. Also, the modes can either appear in the spectrum (bright modes) or will not be visible (dark modes), depending on the magnitude of the net dipole moment.[14] The motivation behind this theory was the fact that, plasmons those are describable by the classical electromagnetic theory have some features resembling electrons in quantum mechanical systems.

This theory decomposes complex plasmonic nanostructures into simple geometries and then studies the possible ways of interaction between them inorder to predict the hybridized plasmon modes of the complex geometry. Such interactions make the resonant wavelength depend on the polarization as well the gap between these structures and results in the generation of extremely large electric fields in these gaps. This finds immense applications in sensing, surface enhanced Raman scattering, photothermal imaging and therapies etc.

Coupling between plasmons in a pair of nanoparticles is the simplest model to explain this. When both the dipoles oscillate in phase with each other, an effective dipole moment will be formed. Depending on the phase generated by the first dipole at the location of second one, the coupled mode gets shifted either to higher or lower frequencies. End-to end arrangement of particles results in an in-phase interaction, which happens at frequencies below the resonance of a single dipole and side-by-side arrangement leads to out-of phase interaction which occurs at higher frequencies. For weak

coupling regimes, only dipolar modes interact with coupled modes, but, for strongly interacting structures, mixing of higher order modes with the coupled mode can also occur.[15]

The description in the original paper is as follows: "In the plasmon hybridization method, the conduction electrons are modelled as a charged, incompressible liquid sitting on top of a rigid, positive charge representing the ion cores. The plasmon modes are self-sustained deformations of the electron liquid. Because the liquid is incompressible, the only effect of such deformations is the appearance of a surface charge."[12]

Starting with the above assumption, for a spherical particle surrounded by air, the potential energy U can be calculated using the spherical harmonics as,[2]

$$U = 2\pi \left(n_0 q\right)^2 \sum_{l,m} N_{lm}^2 \frac{l}{2l+1} \tag{1.9}$$

Here N_{lm} are the amplitudes of spherical harmonic mode (l,m).This equation describes how the interaction between charges define the potential energy and thus the plasmonic behavior. Now, if we consider hybridization between plasmons in a pair of spherical nanoparticles, the interaction energy is given by,

$$U_{12} = \frac{n_0 m_e}{2} \sum_{l_1 m_1, l_2 m_2} U_{l_1 m_1, l_2 m_2} N_{1, l_1 m_1} N_{2, l_2 m_2} \tag{1.10}$$

$$U_{l_1 m_1, l_2 m_2} = \frac{2 n_0 q_2}{m_e} \sqrt{l_1 l_2 R_{s,1} R_{s,2}} \int \int \frac{1}{\mid r_1 - r_2 \mid} Y_{l_1 m_1}^{(r)}(\Omega_1) Y_{l_2 m_2}^{(r)}(\Omega_2) dS_1 dS_2 \tag{1.11}$$

Here, $R_{s,1}$ and $R_{s,2}$ are the radii of two spheres, and Ω_i represents the solid angle with respect to the center of the ith particle. Though no simple analytical expressions exist for $U_{l_1 m_1, l_2 m_2}$, using symmetry and scaling arguments, we can unveil more information on such coupled systems.As we can see, this equation suggests that modes with different l can be mixed by coupling and it occurs when the separation is small.In this case, since the system is cylindrically symmetric with respect to the connecting axis of two particles, m is a conserved quantity and hence there will be no mixing between

11

modes with different m values.For a symmetric nanoparticle pair, bonding and antibonding modes are of opposite parity and hence never couple. But, when they are of different size, such sorts of couplings also take place.

When more than two nanoparticles come together and create a plasmonic molecule, the energy along with the shape of plasmon modes depend on the exact arrangement of particles. Such a scenario can be explained better with the help of group theory taking into consideration point group symmetries, ie, the symmetry adapted linear combinations (SALCs) of individual particle states, from molecular spectroscopy.[14] Moreover, symmetry breaking introduces further more complicated effects life Fano resonances (asymmetric line-shapes in scattering spectra) in particular systems.[16]

1.5   Plasmonic nanoantennas

Antennas are converters between electromagnetic radiation and electrical signals.[17] They are very important in the context of telecommunication and data transfer applications.[18] The concept of antennas are well established in radiofrequency and microwave regimes, but the optical analogue of it has not came into realization for a long time mainly due to the difficulties in fabrication of nanostructures. This was despite the fact that, the prediction of metallic nanostructures as optical antennas was suggested in 1928 by Edward Hutchinson Synge. Later in 1985, John Wessel demonstrated that a metallic nanoparticle indeed acts as an antenna.[19] Recent breakthroughs in the field of nanoscience have helped to circumvent the problem of nanofabrication and currently, plasmonic nanoantennas are an important field of research.[19−27]

Antenna can either be a receiving one or transmitting one and any nanoantenna can act as a receiver as well as a transmitter, as per the principle of reciprocity.[17] A receiving antenna converts electromagnetic radiation into a highly confined field and a transmitting antenna does the other way around. Two important features need to be considered in this context are the efficiency and the emission directionality of nanoantennas. The directivity factor is defined by the equation,

$$D(\theta, \phi) = \frac{4\pi p(\theta, \phi)}{P_{rad}} \tag{1.12}$$

where, P_{rad} represents the total power radiated into the far-field.The total power can obtained by the integration of angular distribution of power p

(θ,ϕ) over the whole surface. Here,(θ,ϕ) are the angular co-ordinates of the spherical co-ordinate system.

Having emission patterns in a particular direction and only in that direction (unidirectional emission) becomes crucial in location-specific information transfer in optical chips.

Chapter 2

Methods

This chapter presents the methods involved in this work. Discussions on seed-mediated synthesis method of gold nanorods and the numerical techniques employed to perform electrodynamical calculations are included.

2.1   Numerical Methods

Near-field and far-field optical properties of metallic nanostructures of arbitrary geometries can be calculated by a variety of electrodynamic based numerical techniques like the finite-difference time-domain (FDTD), the discrete dipole approximation (DDA)[4,28], the finite element method (FEM)[29,30], the multiple multipole (MMP) method, the boundary element method (BEM), plane wave expansions and transfer-matrix approaches. The flexibility of modelling systems and sources of our interest in different environments, which is difficult when accessed using experiments, makes them good platforms for gaining a deeper insight into how electromagnetic waves interact with matter.[30]

For the studies on extended wavelength scale objects and nanoparticle arrays, transfer matrix approaches and plane wave expansions work well. But, in the case of nanometer-scale subwavelength individual particles of arbitrary geometry or closely spaced nanoparticles, such techniques become difficult to apply and we need to use real-space methods such as FDTD, DDA, FEM, BEM or MMP method. In our study, we have utilized FDTD approach to calculate near- and far-field optical properties of gold nanorod dimers of various orientations.

2.1.1 Finite Difference Time Domain (FDTD)

FDTD is a grid-based differential numerical modelling method. The basis of this technique is the two Maxwell curl equations in derivative form in the time domain. Maxwell's equations are solved numerically within a finite computational space that has been divided into cells. The electromagnetic fields are discretized in time and space on a grid that contains the material to be studied and a surrounding environment where the response is to be determined. Any material can be used as far as we know its permittivity, permeability and conductivity. Field can be determined explicitly by propagating discrete versions of Maxwell's equations forward in time. The electric and magnetic field can be calculated at every point within the computational region upon feeding the appropriate boundary conditions.

Incident field

The incident field can be specified in many different ways, one being the total-field scattered-field (TFSF) method. In this case, the computational region is divided into two separate regions; the first region contains the total field which has the incident field and the scattered field, and the second region comprises of only the scattered field. The wavevector of the incident field which is a plane wave is normal to the surface. This method is particularly useful for the studies on scattering from objects, as the scattering field can be isolated from the incident field.

Boundary conditions

We have to make sure that when the field scattered from the objects reach the boundary, they should feel the computational space to be infinite. But, the space we define in FDTD is essentially finite. In order to take into account this, we can use a boundary condition called the perfectly matched layer (PML) absorbing boundary condition. These layers absorb light waves with minimal reflections. So, when the outgoing waves reach the boundary, the space appears infinite to them.

Far-field properties

FDTD calculations generally give information about near-field properties such as the electric and magnetic fields within the computational space. However, often we are also interested in knowing far-field properties such as scattering cross-sections and angular distribution of reflected light from metallic nanostructures, which requires calculating the fields everywhere in

the far field. Fortunately, it is possible to do so in FDTD with the help of in-built analysis groups, if the incident field has a sinusoidal time dependence.

2.2 Fourier/Back focal plane(BFP) imaging

Probing the optical properties of systems generally involve the investigation of size, position and wavelength and intensity of the underlying object. It is equally important to know the direction of light emission or scattering from those objects. To extract information about, which angle the light is been scattered, a method called Fourier plane imaging or back focal plane imaging is used. Here, the back focal plane of the objective lens gives information about the directivity of light emission from the system under consideration.

For an emitter in a uniform environment, the emission angles will be determined only by the inherent properties of that emitter and it will not have any contribution from the surrounding medium. If we consider a point dipole in a homogeneous medium of dielectric constant n_1, the emission would be that of a free space Hertzian dipole model, which means that, it would be radially symmetric with respect to the axis parallel to the effective dipole moment, with the highest intensity into the angles perpendicular to the dipole axis. But, upon placing this emitter on a medium having refractive index n_2, surrounded by a dielectric with refractive index n_1, where $n_1 < n_2$, radiation pattern changes. This situation can be imagined as follows: Consider an emitter placed on a glass cover slip which is been illuminated by a high numerical aperture objective lens. If θ is the angle of emission, and E_{emit} is the electric field generated by the emitter, then the intensity distribution in the Fourier plane of the objective lens can be expressed as

$$I_{BFP} \propto 1/\cos(\theta) \, |E_{emit}|$$
(2.1)

2.3 Dark field optical microscopy

Dark field optical microscopy is a far-field technique, where the only light scattered by the nanoparticle is collected, excluding the unscattered light. It facilitates so by using a dark-field condenser which blocks the collection of directly transmitted light, due to which the field around the particle appears dark. Hence, nanoparticles appears in bright colours which is determined by their resonance wavelengths. As the resonance wavelength is a function of

nanoparticle size, geometry and orientation, the colours in dark-field images gives information about the geometrical parameters of the nano-objects.

2.4 Synthesis of gold nanorods(Au NRs)

We have chosen to use bottom-up methods for the synthesis of gold nanorods (Au NRs) due to the single-crystallinity of the NRs we end up with. This can, in general be performed either in the presence of a neutral/ charged surfactant or in a rigid template. Hexadecyltrimethylammonium bromide (CTAB) is a commonly used surfactant in aqueous media syntheses of gold and silver nanoparticles. In our work, Au NRs were synthesized by seed-mediated surfactant-directed growth method with CTAB as the surfactant, as proposed by El-Sayed.[32]

2.4.1 Chemicals used

Gold chloride trihydrate ($HAuCl_4.3H_2O$), hexadecyltrimethylammonium bromide (CTAB), sodium borohydride ($NaBH_4$), ascorbic acid, silver nitrate ($AgNO_3$), 5,5′ bis(mercaptomethyl)-2,2′-bipyridine and milli-Q water. All the chemicals were purchased from *Sigma Aldrich*.

2.4.2 Preparation of seed solution

5 ml of CTAB solution (0.2 M) was added to the same amount of $HAuCl_4.3H_2O$ (0.0005 M) and stirred it well. After stirring, 0.6 ml of ice-cold $NaBH_4$ (0.01 M) was added to the solution which gave rise to a brownish yellow solution. This surfactant-capped seed solution was maintained at a temperature of 25°C after vigorously stirring it for 2 minutes.

2.4.3 Preparation of growth solution

5 ml of CTAB solution (0.2 M) was gently mixed with 0.2 ml of $AgNO_3$ (0.004 M) at 25°C. followed by the addition of 5 ml of $HAuCl_4.3H_2O$ (0.001 M) which produced a dark yellow color. After gentle mixing, 70 μl of ascorbic acid, a mild reducing agent was added which turned the solution to colorless.

2.4.4 How are Au NRs formed?

Upon adding 12 μl of the seed solution to the growth solution at 28° C, a gradual change in color to violet was observed in about 30 minutes. This

solution containing NRs were double-centrifuged at 8000 rpm for 20 minutes to remove excess CTAB and diluted with milli-Q water after sonication.

Two possible mechanisms has been proposed to explain the growth of Au NRs. One suggests that, the role of surfactant is to act as a soft template which facilitates the diffusion of Au atoms onto it. The size of the template varies as a function of the concentration of the surfactant as well the ionic strength of the solution. When seed solution is been added to the growth solution, the seed becomes part of the template and growth happens by the diffusion of Au atoms to the template, as mentioned above. As per the other possible mechanism, the seed which is surfactant-capped starts its growth and then more atoms join the crystal lattice, those are protected by the surfactant monomers. Ascorbic acid is a mild reducing agent which selectively reduces gold ions, even though the growth solution contains both gold and silver ions. Silver ions get reduced by ascorbic acid only if the medium is of basic pH. It has been reported that, NRs gets converted into nanospheres if the synthesis is done in the absence of silver ions, which points out the fact that silver ions essentially gets adsorbed at the Au nanoparticle surface as $AgBr$ which restricts the growth and thereby stabilizes the surface of NR.

The aspect ratio of the NRs can be varied by changing the concentration of Au atoms in the growth solution. This is also a function of the concentration of silver ions, those are shown to have a catalytic effect on the growth of Au NRs. At the same time, it has also observed that, higher concentration of $AgNO_3$ results in decreasing the length of rods, which could be attributed to ionic strength effect.[36−38] However, the question of, why the length of NR is getting increased with Ag ion concentration is still not clearly understood.

2.4.5 Assembly as dimers and trimers in solution

It is known from Zeta potential measurements that, Au NRs are stable for a significant number of hours in a solvent mixture of water and acetonitrile, which contains more than 70 % of acetonitrile.[33−35] In our case, we have used a solvent mixture of 1: 4 water: acetonitrile (500 μl: 2000 μl) containing NRs. 160 μl of dithiol molecule (5, 5′ bis(mercaptomethyl)-2,2′-bipyridine (160μM)) in acetonitrile was added as the linker group, which facilitates dimerization as well as higher order self-assembled structures. When the solvent is rich with acetonitrile, the end facets of the NR are less saturated with CTAB than those were in water. Upon the addition of dithiol molecules, one of these thiol groups binds to the edges of the NRs while the other end remains free. Therefore, dimerization and oligomerization happens only

above a critical concentration of thiol molecules.

Chapter 3

Results and Discussions

This chapter presents the results obtained from the characterization of gold nanorods and from the electrodynamical calculations done using the software 'Lumerical FDTD Solutions' and the subsequent discussions. Microscopy images, UV-Vis spectrum, scattering spectra, near-field and far-field radiation patterns obtained for single and dimeric gold nanorods - both, on the substrate and without the substrate are shown in the subsections of this chapter.

3.1 Synthesis of single-crystalline gold nanorods and their characterization

Single crystalline Au NRs were synthesized by the seed -mediated surfactant-directed growth method, which is described in the chapter $2^{[32]}$ and they were characterized by UV-Vis absorption spectroscopy, field emission scanning electron microscopy (FE-SEM), transmission electron microscopy (TEM) and dark field optical microscopy. The nanorod solution had a bright violet color and the UV-Visible spectrum of NRs exhibited two distinct peaks at 528 nm and 742 nm, see figure 3.1. The intense peak at the higher wavelength corresponds to the longitudinal mode resonance and the less intense one at a lower wavelength to the transverse mode resonance. The diluted sample of NRs was drop-casted on a clean glass slide and on silicon substrates for visualization under dark-field microscopy and FE-SEM respectively. The average dimensions of NRs in the solution was determined from SEM images, which was about 60 nm in length and 20 nm diameter. Images captured under SEM and TEM showed well-dispersed isolated Au NRs (figure 3.2 and 3.3). After obtaining such monomers, dithiol molecules were used as linker molecules to achieve assemblies of nanorods.The resultant solution had few dimers, trimers and higher order structures; but those were difficult to well
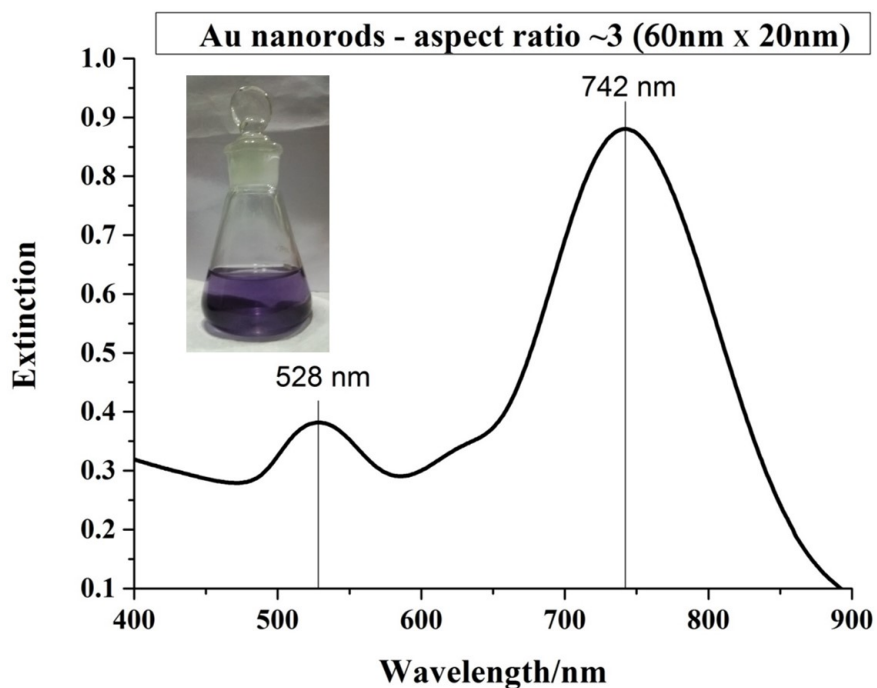
Figure 3.1: *UV-Vis spectrum of the gold nanorod solution showing transverse peak at 528 nm and longitudinal peak at 742 nm; photograph of the solution is shown in inset, which is having a bright violet colour.*
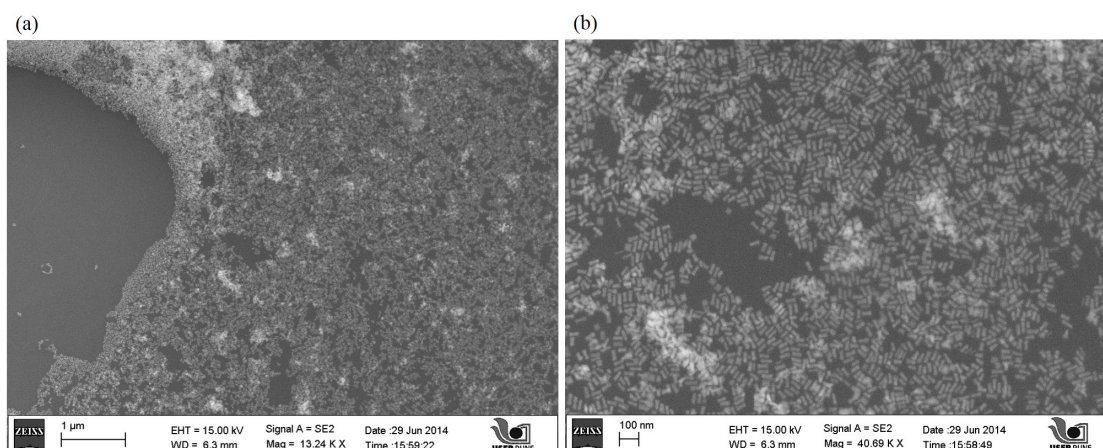

Figure 3.2: *FE-SEM images of well dispersed gold nanorods. The scale bar in (a) is 1 μm and (b) is 100 nm.*
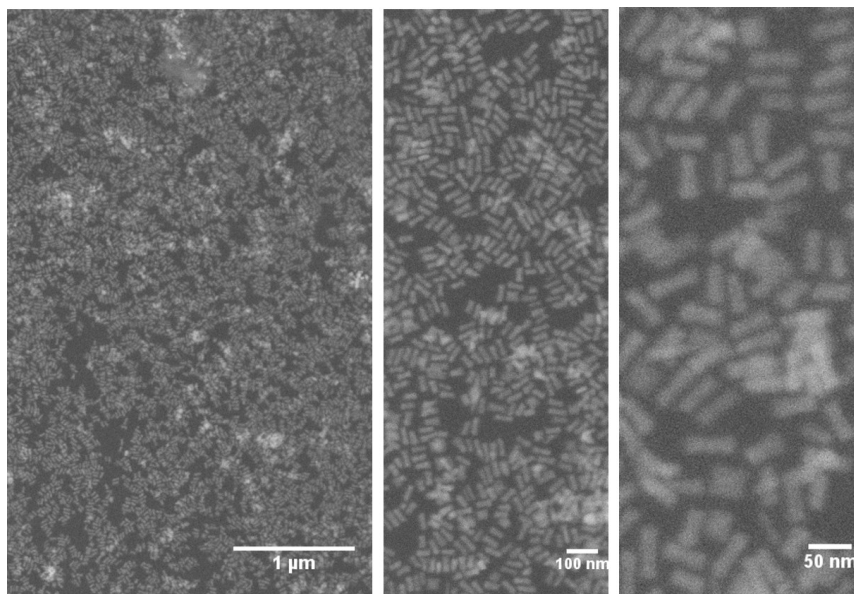
21

Figure 3.3: *FE-SEM images of monodispersed gold nanorods with scale bars 1 µm, 100 nm and 50 nm.*
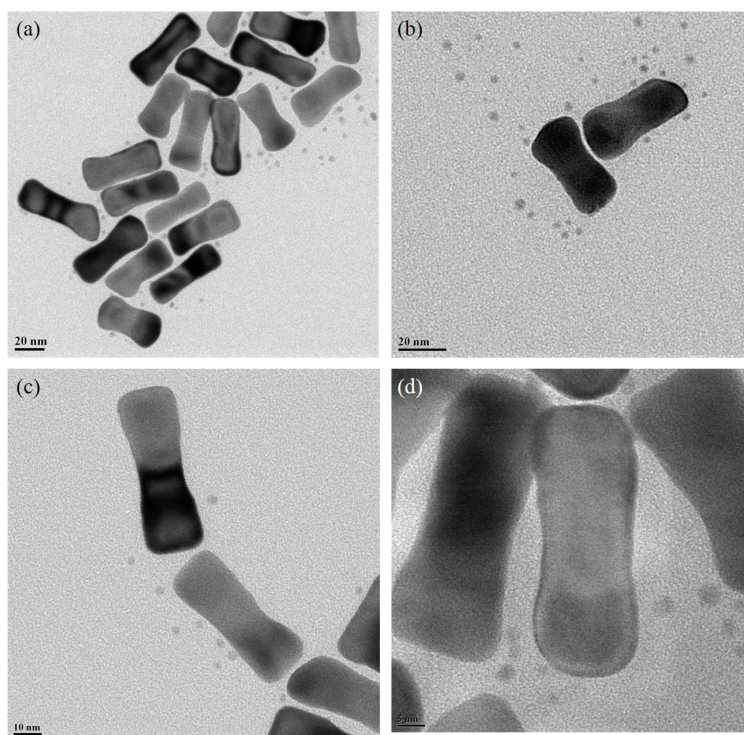

Figure 3.4: *TEM images of (a) monodispersed gold nanorods, (b) a T shaped dimer, (c) an angled dimer and (d) a touching dimer.*

resolve in FE-SEM. TEM images of a monomer sample and few dimers is shown in figure 3.4.

3.2   Single nanorod scattering spectra

Studies on optical properties of single nanostructures are of immense interest in the context of sensing, labelling, optical antennas, optical trapping, biochemical applications etc.[36−46] The scattering spectra of single plasmonic nanostructures inevitably provide a lot of insight into the behaviour of plasmonic modes at different frequencies. In this section we explore the dependence of scattering cross-section on the aspect ratios of single nanorods in a homogeneous medium as well as on a supported glass (SiO_2) substrate. All the spectra were calculated using 'Lumerical FDTD Solutions software, using a total-field scattered field (TFSF) source and perfectly matching layer boundary (PML) conditions. The nanorod was modelled as a cylinder having hemispherical end-caps with a dielectric constant defined by Johnson and Christy[47] and the dielectric constant of SiO_2 was taken from Palik.[48]

3.2.1   Effect of aspect ratio - Unsupported nanorod monomers

Inorder to understand the effect of dimensions of nanorods on the scattering behavior, spectra has been calculated for a series of nanorods with different dimensions in a homogeneous environment of refractive index 1 (air). Initially the length of the rod has changed from 20 nm to 90 nm for a fixed diameter of 20 nm. Spectra has been calculated for two different excitation polarizations-parallel to the long axis of the nanorod and perpendicular to it. Obtained spectra are shown in the figure 3.5. A gradual redshift is seen with an increase in length for parallel polarization (p pol) which is exciting the longitudinal plasmon mode, whereas the perpendicular polarization (s pol) excites the transverse mode which does not show significant shift with a change in the length of the rod.

As the next step, the length was kept fixed as 60 nm and the diameter was varied from 60 nm to 13.33 nm so as to span aspect rations from 1 to 4.5 (figure 3.6). Trend for longitudinal excitation is similar to the case when the length was varied, but the intensity profile does not show a well-defined pattern. The position of transverse peak is redshifted when the symmetry is broken from spherical to an anisotropic structure. Apart from that, s polarized light did not cause any observable difference in the scattering spectra.
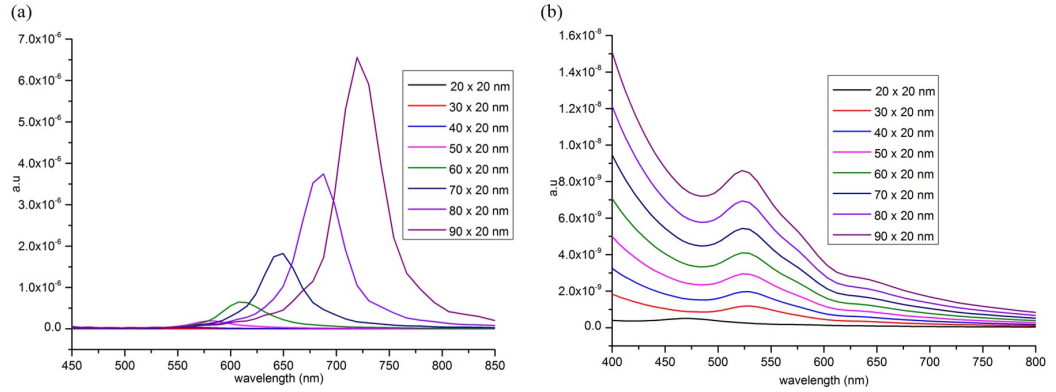
Figure 3.5: *Scattering spectra of Au NRs of a fixed diameter of 20 nm with lengths 20 nm (spherical), 30 nm, 40 nm, 50 nm, 60 nm, 70 nm, 80 nm and 90 nm upon illumination with (a) p- polarized light. (b) s-polarized light.*
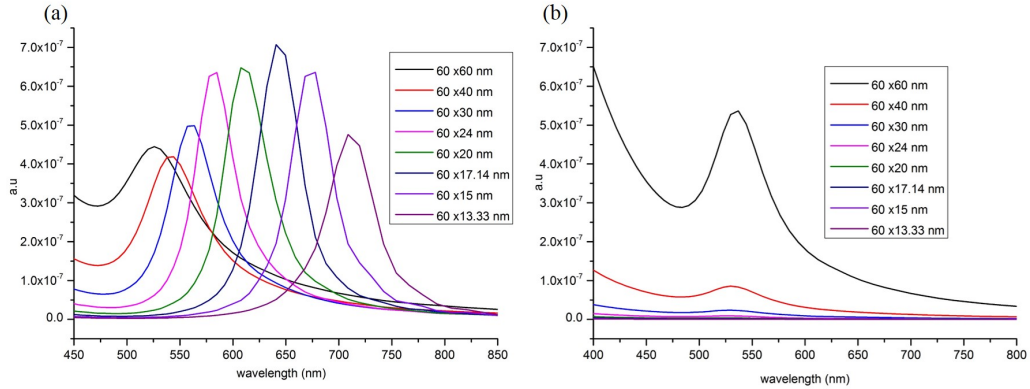

Figure 3.6: *Scattering spectra of Au NRs of a fixed length 60 nm with diameters 60 nm (spherical), 40 nm, 30 nm, 24 nm, 20 nm, 17.14 nm, 15 nm and 13.33 nm, upon illumination with (a) p- polarized light. (b) s-polarized light.*

The conclusion drawn is that, the longitudinal mode is sensitive to the change in the dimensions of the nanorod. On the other hand, transverse mode does not gets affected much, atleast to the extent where the shift is observable in scattering spectra. Hence the longitudinal plasmon band position is plotted as a function of aspect ratio for both the above cases and a linear relationship is obtained as expected.[15] Peak positions got shifted to higher wavelengths and thus to lower energies with an increase in aspect ratio.
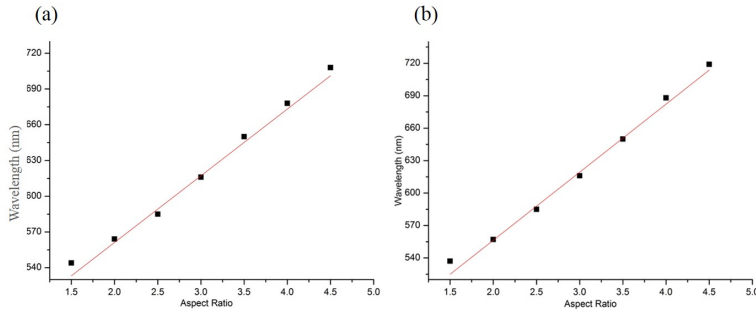
Figure 3.7: *Longitudinal plasmon band position as a function of rod aspect ratio when the (a) length is varied, (b) diameter is varied.*

Here, it should be noted that the details of the NR geometry also plays a critical role in determining the peak position. For example, in our case, the nanorod was cylindrically symmetric. If the end faces are rectangular and not curved or if they are ellipsoidal, then the scattering behaviour will be significantly different from what was obtained here.

3.2.2 Supported nanorod monomers

Optical properties are very sensitive to the changes in the effective environment of the plasmonic material. To understand near-field and far- field properties of gold nanorods in experimental environments, they were considered to be on a supported substrate. For all further investigations, the nanorod dimensions are chosen to be 60 nm in length and 20 nm in diameter as it was the dimension obtained from our synthesis method. They were placed on a glass substrate and is illuminated with a light source through the glass; the schematic for this system is shown in the figure 3.8 (a).

To begin with, parallel polarized light was used for illumination and scattering spectra was collected. The peak position 662.5 nm was significantly red shifted from the 616 nm which was the peak value for unsupported case. Here, the rods are experiencing a completely different environment which is not homogeneous, so symmetry is broken in one more dimension.Note that the nanorod is resting on a glass substrate with its long axis parallel to the glass. Calculated near-field intensity profiles for both the polarizations are shown in the figure 3.8 (b) and (c).
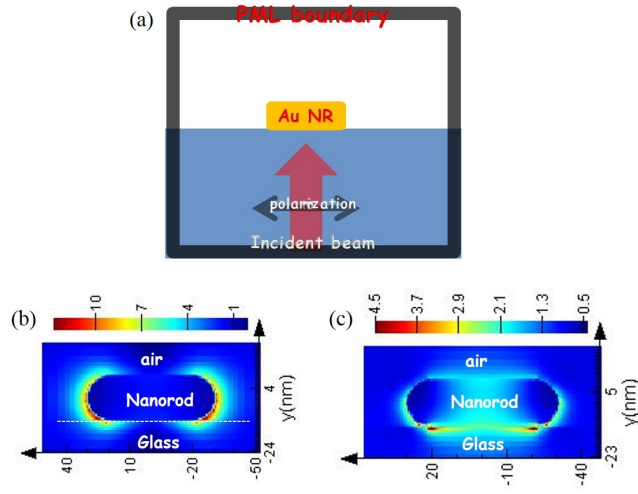
Figure 3.8: *(a) Schematic of a FDTD simulation for a supported gold nanorod. The near-field intensity distribution for a polarization (b) parallel (c) and perpendicular with respect to the long axis of the rod is shown.*
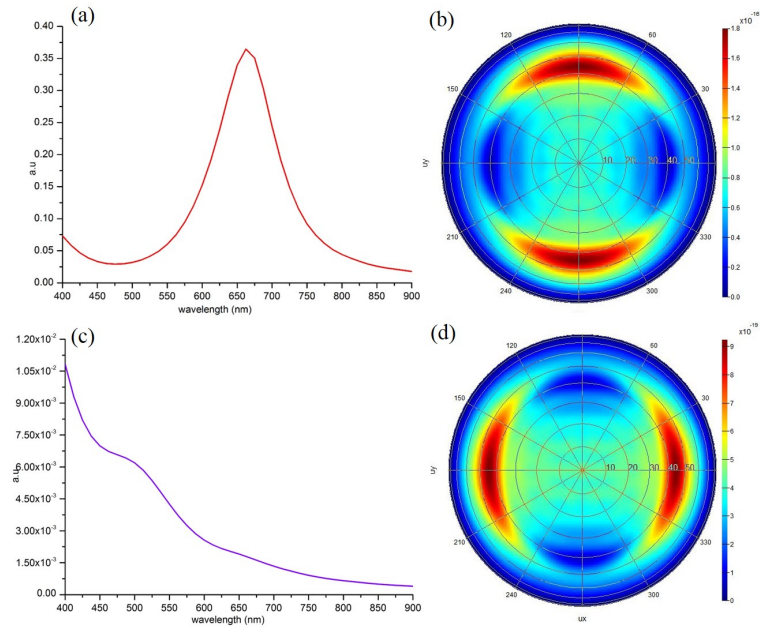

Figure 3.9: *Scattering spectrum for a supported gold nanorod for an excitation polarization of (a) 0° (c) 90° and the corresponding far-field projections. The direction of emission at 90° polarization is orthogonal to the 0° case.*

The difference in the locations of high field intensities for these two cases

are evident from these figures.Then far-field radiation patterns were extracted from the built-in far-field projection calculator of the FDTD solver and the plot of intensity as a function of the azimuthal angle ϕ was obtained. Scattering spectra and far-field radiation patterns for polarizations $0°$ and $90°$ are shown in figure 3.9. As expected, the far-field projection with perpendicular polarization was orthogonal to that with parallel polarization. For both these cases, far-field patterns were calculated with different excitation wavelengths, but no significant change was observed.Thereafter, similar calculation was done with illumination polarizations $45°$ and $135°$ (figure 3.10).
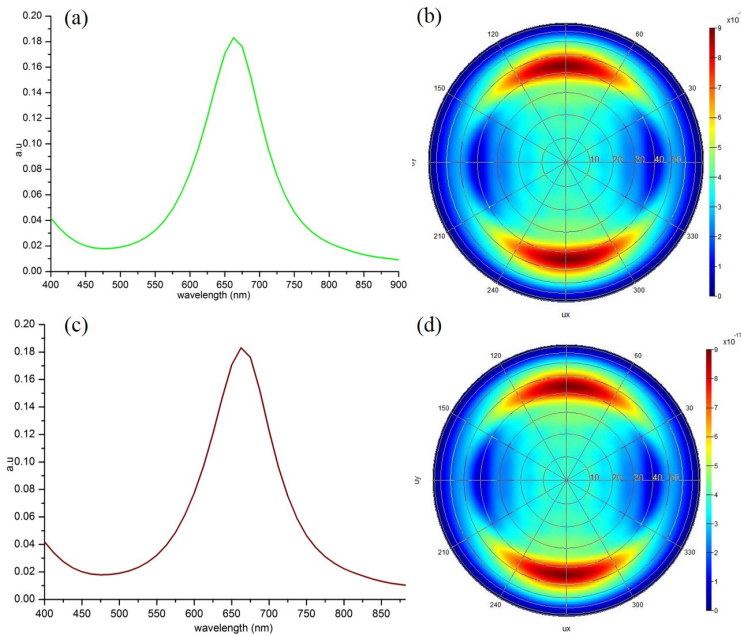

Figure 3.10: *Scattering spectrum for a supported gold nanorod for an excitation polarization of (a) $45°$ (c) $135°$ and the corresponding far-field projections. The direction of emission is similar to that of $0°$ case*

The peak position remained the same and at the peak excitation wavelength, the far-field image has similar directions of emission as the $0°$ case. But, interestingly, at other excitation wavelengths, positions of dipolar lobes changed. This essentially means that, even though the plasmon mode peak resonances of supported single nanorods are the same for two different polarization vectors, their far-field projections may vary significantly (figure 3.11).
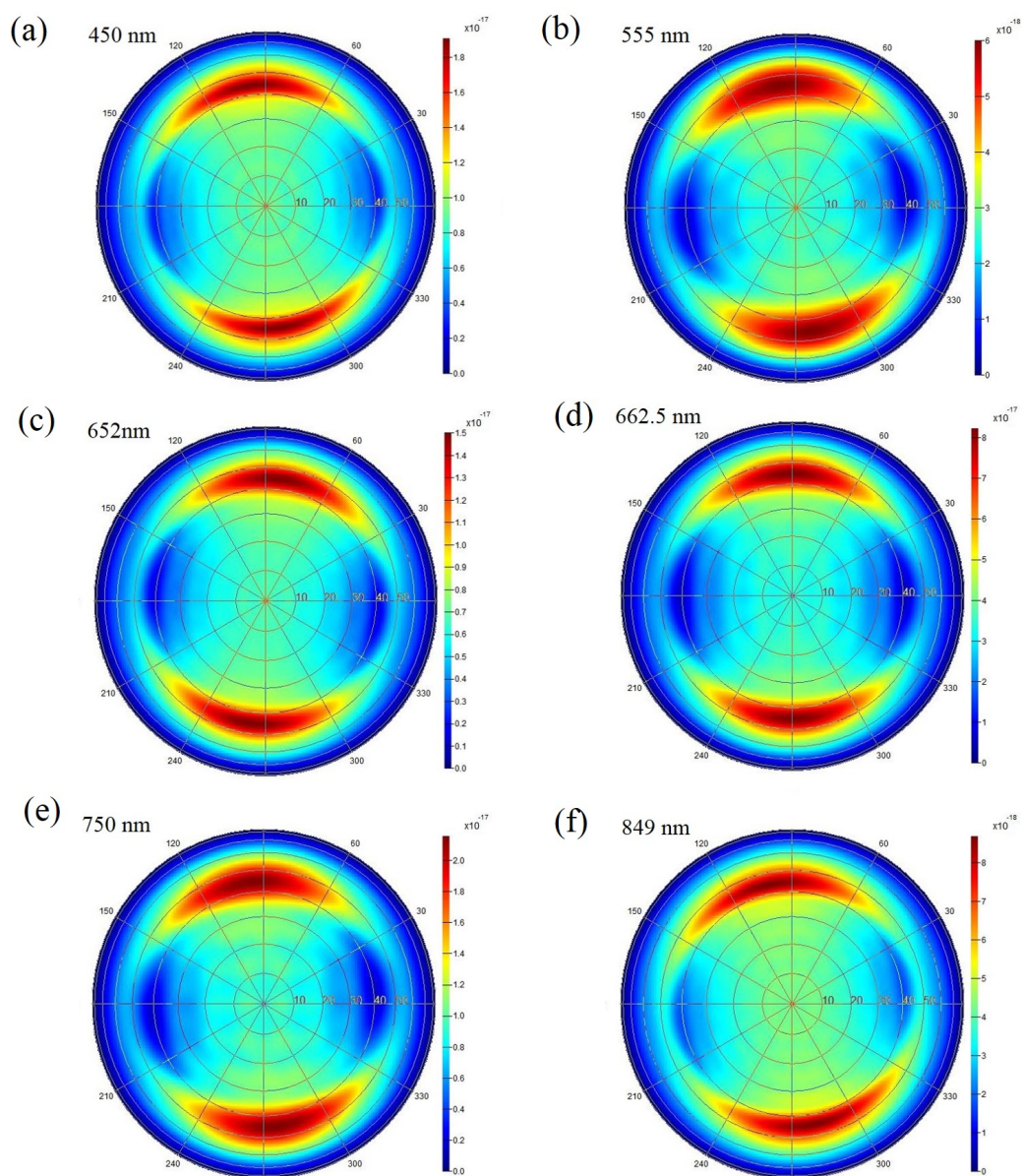
Figure 3.11: *Far-field radiation patterns for a supported gold nanorod having polarization vector of electric field at an angle 45° at excitation wavelengths at (a) 450 nm (b)555 nm (c) 652 nm (d) 662.5 nm (e) 750 nm and (f)849 nm*

This observation will have direct implications in utilizing gold nanorods as optical antennas.

3.3 Nanorod dimers

Plasmon coupling between nanostructures can be understood by plasmon hybridization theory which was described in chapter 1.The shape anisotropy of nanorods enables a variety of orientational possibilities, which helps us to gain further insight into the coupling mechanisms. Near-field coupling interactions result in the shift of energy levels into either higher (anti-bonding) or lower (bonding) wavelengths depending on the orientation, gap widths, polarization etc. Here, end-to-end coupled (180°), side-by-side aligned (0°) and angled symmetric nanorod dimers with small interparticle distances (upto 7 nm) are chosen for studies.

3.3.1 End-to-end coupled nanorods

To begin with, unsupported nanorods dimers, each having dimensions of 60 nm x 20 nm arranged in end-to-end fashion were chosen. Scattering spectra were calculated for different separations starting from 0 nanometers to 5 nanometers with a polarization parallel and perpendicular with respect to the long axis (figure 3.12).
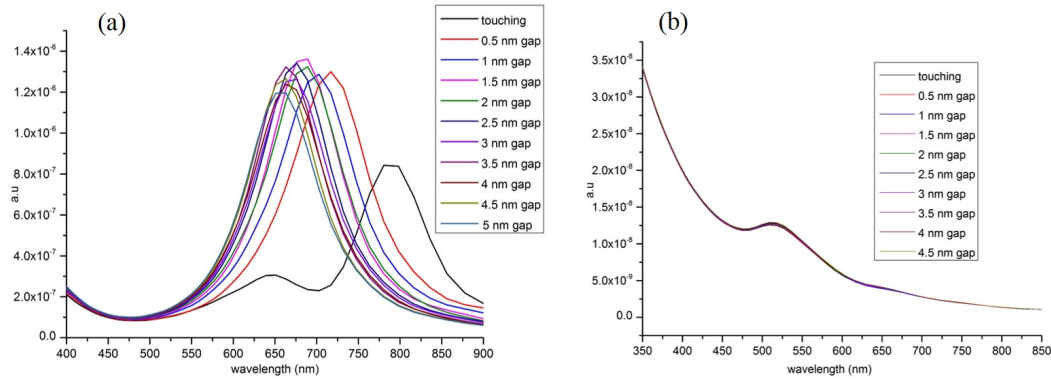

Figure 3.12: *Scattering spectra of end-to-end coupled unsupported gold nanorods for different gap sizes shown in the inset, for polarization (a) parallel to the long axis (b) parallel to the long axis.*

Coupled longitudinal modes in such systems result in bonding type interactions (attractive coupling) which can be confirmed from the spectra by an increase in energy of the LSP mode. Note that the touching nanorod geometry has two peaks in the span of shown wavelengths in the spectrum.

The less intense mode at lower wavelength corresponds to the higher order mode and for non-zero gap sizes, it begins to appear at further lower wavelengths. When gap size increases, the coupling strength becomes weaker and the peak position gets slightly redshifted for small separations. With further increase in separation, no significant change happens for the scattering maxima. Coupled transverse modes get excited for perpendicular polarizations and no change in the spectra was observed for varying separations, which can be attributed to weak coupling scenario.

Upon introducing glass substrate and exciting with parallel polarization, similar trend was observed, but for the touching dimers, there was a drastic reduction in the intensity of longitudinal peak which is shown in figure 3.13.
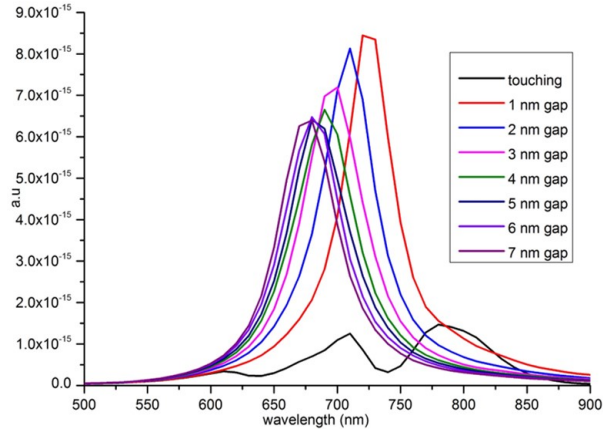

Figure 3.13: *Scattering spectra of end-to-end coupled Au NRs resting on SiO_2 for different gap sizes shown in the inset, for polarization parallel to the long axis.*

3.3.2 Side-by-side aligned nanorods

Scattering spectra are calculated for nanorods aligned in side-by side fashion, by keeping a polarization parallel to the length of rods and thus perpendicular to the gap. For such orientations, coupling of longitudinal and transverse modes happens similar to antibonding interactions. The polarization vector here is essentially exciting the transverse mode and hence the peak position is slightly redshifted from that of a single monomer. Nevertheless, information regarding the variation in gap size is not evident from the scattering spectra obtained, since the peak value is more or less the same for all investigated gap widths upto 5 nm (figure 3.14). Inorder to extract more information
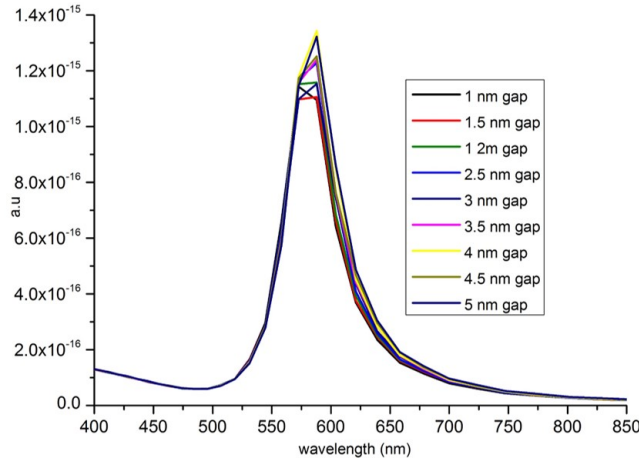
Figure 3.14: *Scattering spectra of side-by-side aligned Au NRs resting on SiO$_2$ for different gap sizes shown in the inset, for polarization perpendicular to the gap width.*

regarding this aspect, incident light with an orthogonal polarization has to be used.

3.3.3   Angled nanorod dimers - antenna properties

In both the cases above, the chosen orientation allowed selective coupling of longitudinal modes of one nanorod to the similar mode of the other rod. There was no possibility of mixing of transverse and longitudinal modes. If we bring in an angle between nanorods, so that the electric field vector would have polarization components not along either the width or length of individual nanorods, there is a chance of having transverse-longitudinal mode coupling as well.

Here we have considered a dimer system with a fixed gap size of 3 nanometers and varied the angle between them. The gap was defined in such a way that, 3 nm was the shortest distance between the curved end-caps of the nanorods. Scattering spectrum, near-field patterns and the far-field projections at various excitation wavelengths were obtained for angles of 45°, 60°, 90°, 60°, 135° and 180° between nanorods. Firstly, let us consider the case of 45° angled dimer, the schematic of which is shown in figure 3.15 (a). Upon excitation with a source having polarization parallel to the gap, scattering peak occurred at 685 nm.
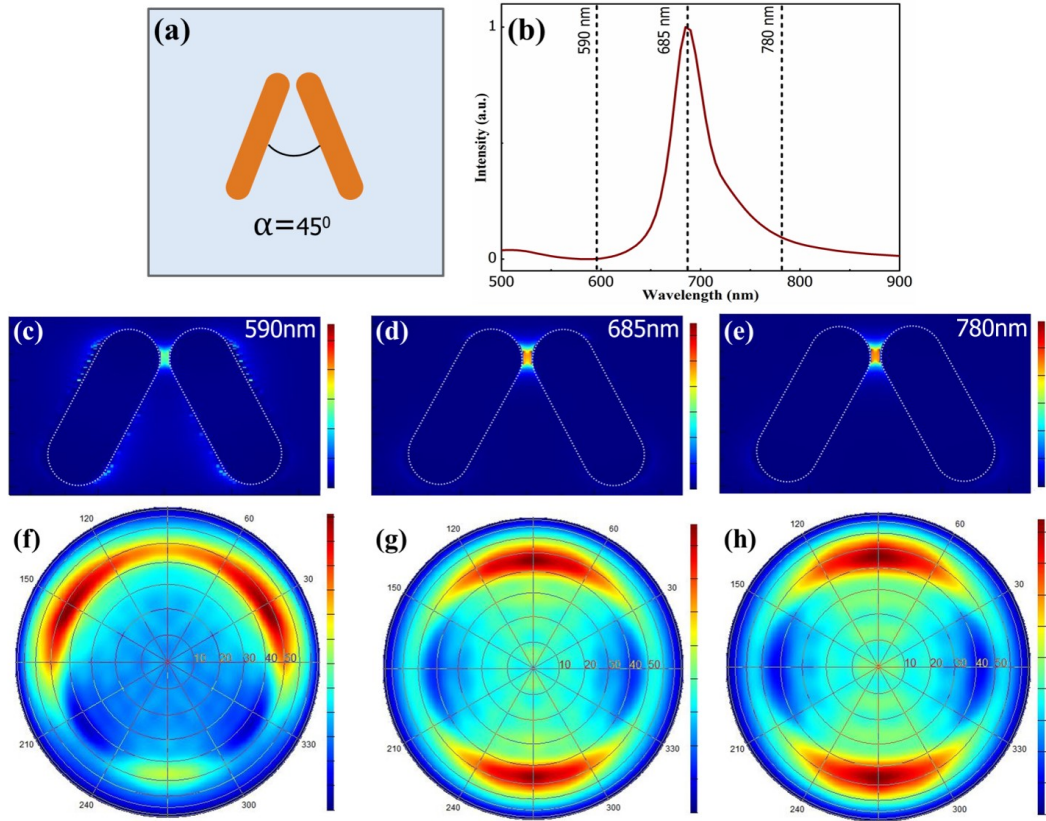
Figure 3.15: *(a) 2-D geometry of a nanorod dimer with 45° angle and 3 nm gap with excitation polarization parallel to the gap.(b) Simulated scattering spectrum for this geometry which shows a peak wavelength of 685 nm. The asymmetric nature of the curve resembles Fano interference pattern which in turn results in a minimum at 590 nm (marked with dotted line). (c), (d) and (e) are the near-field intensity distributions at the Fano dip, scattering maximum (685 nm) and at a red-shifted region (780 nm); it is clear that the near-field intensity distribution is very much different at the 590 nm although the intensity is lower than the other two wavelengths. (f), (g) and (h) are the projected plots of far-field intensity, at all these three wavelengths. The far-field pattern for 590 nm exhibits a split in the emission pattern which is an indicator of bi-directionality (the scattering intensity is almost negligible at its symmetrically opposite directions) whose signature is not present at the other two regions. The colour scale bars for all the images represent the electric field intensity where, red measures the maximum value and blue, the minimum.*

It is to be noted that, the line-shape is asymmetric and it resembles a Fano-like line-profile having a dip at 590 nm. The near-field intensity distributions at the peak wavelength and at the Fano-dip are shown in figure 3.15 (c) and (d) and the corresponding far-field projections in figures 3.15 (f) and (g) respectively. Unlike the case at scattering peak where the maximum near-field intensity is concentrated at the gap between two nanorods, at the Fano-dip, it is mostly toward the edges of the rods. This anomaly was also reflected in the far-filed pattern at the Fano-dip wavelength which shows a split in the emission pattern which points towards bi-directionality. Inorder to see what happens at a wavelength which is at the red-side of the spectrum, we chose a wavelength of 780 nm and calculated near- and fa-field patterns. They were essentially similar to the case at the peak wavelength. We also checked these patterns at other wavelengths near the scattering peak, at the red-side and near the Fano-dip. The signature of bidirectionality was present from 500 nm to 640 nm, but was more pronounced at the dip wavelength, whereas for all the other regions of the spectrum, the emission was dipolar. From this, we can speculate that there is an intrinsic connection between the Fano-dip in the spectrum and the directionality of far-field emission.

Furthermore, similar calculations were done with a polarization perpendicular to the gap width, the schematic of which is shown in the figure 3.16 (a). The scattering spectrum has a peak at 620 nm (figure 3.16 (b)) which is blue-shifted from the above case and the line-shape was symmetric. As there was no dip in the spectrum, we chose two regions those are 100 nm away from the peak position (marked as dotted lines in the figure 3.16 (b)) and calculated near- and far-field properties (figure 3.16 (c) to (h)). Though the near-field distributions were different for these investigated regions, the far-field projections were similar. The same for other wavelengths were also investigated and no significant difference was observed.

As the next step, dimers with 60° and 180° inter-rod angles were considered, the results of which are shown in the figure 3.17. Scattering peak value for 60° was at 706 nm (a) and for 180°, 700 nm (h). Also the line-shape of the spectrum for 60° inter-rod angled dimer was a little asymmetric. For this geometry, similar to the previous case, near-field and far-field patterns at the dip-wavelength, peak wavelength and at a longer wavelength region were considered. Again, the near-field distribution was different at the dip-like region compared to the other two regions and this reflected in the far-field projection as an increased spread of ϕ in one direction. In this case, the spectral dip is not as prominent as in the case of 45° angled dimer; not having a split in the ϕ spread can be attributed to this fact.For end-to-end coupled

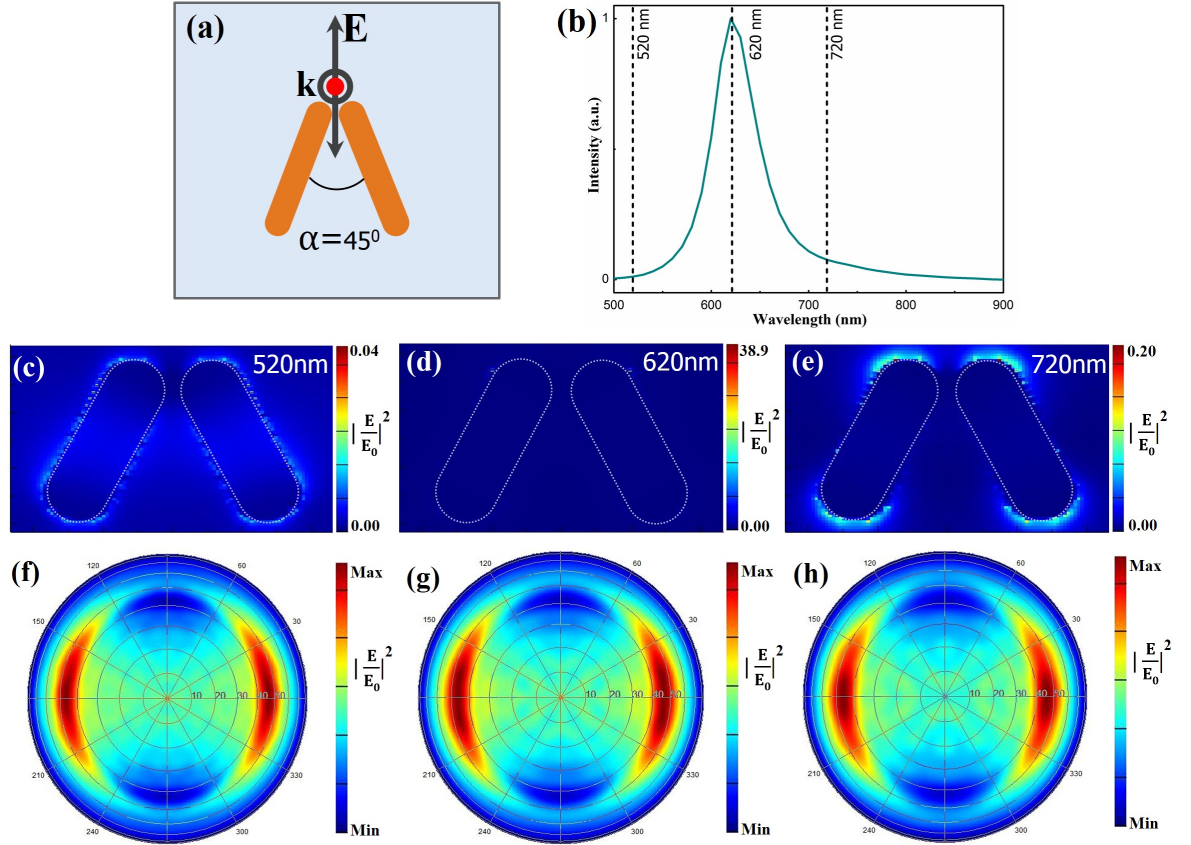dimer, all the three regions exhibited similar field distributions.

Figure 3.16: *(a) 2-D geometry of a nanorod dimer with 45° angle and 3 nm gap with excitation polarization perpendicular to the gap.(b) Simulated scattering spectrum for this geometry which shows a peak wavelength of 620 nm. (c), (d) and (e) are the near-field intensity distributions at 520 nm, scattering maximum and at 720 nm; it is clear that the near-field intensity distributions are significantly different at these three wavelengths. (f), (g) and (h) are the projected plots of far-field intensity, at all these three wavelengths. Unlike the difference in near-field intensity distribution, far-field patterns are similar at all these three regions The colour scale bars for all the images represent the electric field intensity where, red measures the maximum value and blue, the minimum.*
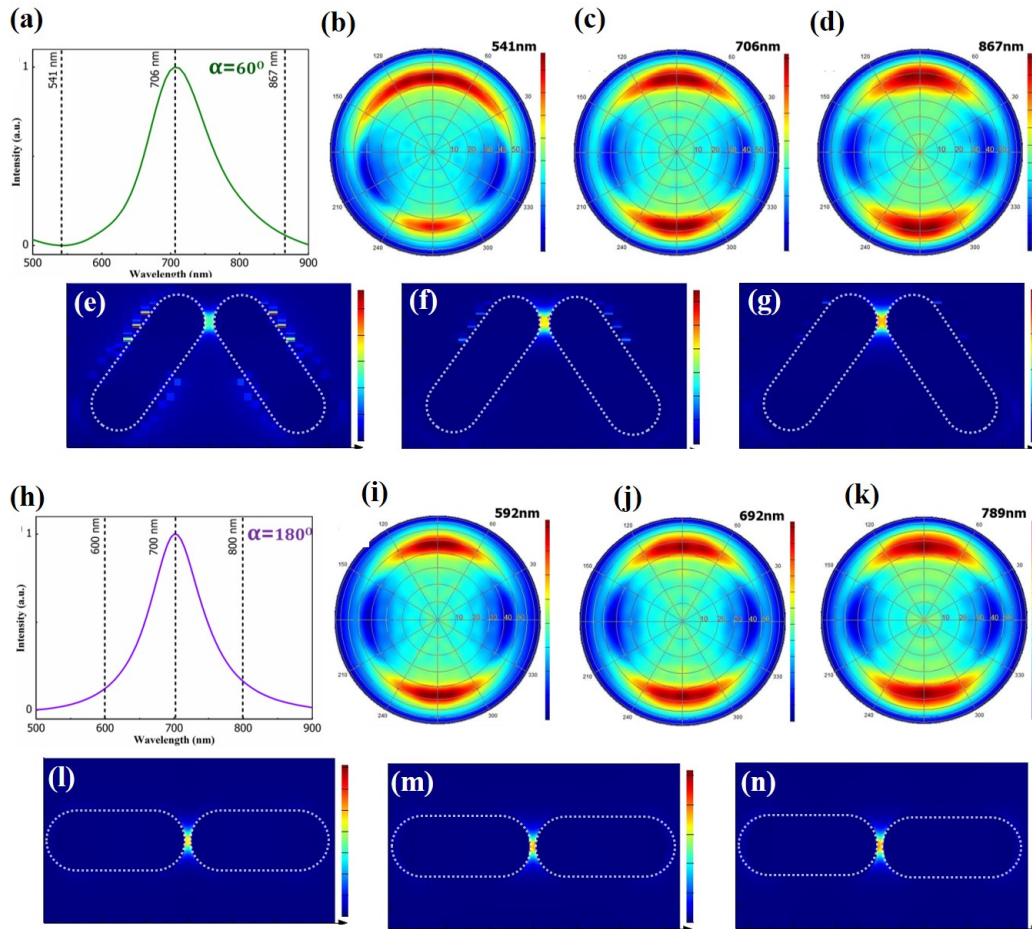
Figure 3.17: *Simulated scattering spectra for gold nanorod dimers having 3 nm inter-rod gap, with two different angles (a) 60° (h) 180° (end-to-end connected). 60° geometry shows a little asymmetric spectral line shape which is not evident in the case of linear geometry.(b) to (d) and (l) to (n) are the corresponding far field projection patters for these geometries at three different wavelength regions (marked as dotted lines in the scattering plots). We can see the increased spread of φ, in particular at one direction (with a higher scattering intensity than the other direction) for the 60° angled geometry only at the blue-side of the spectrum. For the linear dimer, far-field patterns are symmetric and no significant change is observed for different wavelength regions. (e), (f) and (g) are the near-field intensity patterns for the 60° angled dimer at those marked wavelengths; (l), (m) and (n) are those for the linear dimer. The colour scale bars for all the images represent the electric field intensity, where red measures the maximum value and blue, the minimum.*

Next, nanorods dimers having an inter-rod angle of 90° (perpendicularly placed) and 135° were considered. The scattering maxima of perpendicular dimers occurred at 682 nm and that of 135° angled at 688 nm, which is a very small shift. The far-field projections at different excitation wavelengths are shown in figure 3.18 and figure 3.19. Excitation wavelengths were varied from 550 nm to 850 nm and the corresponding emission patterns from the nanorods were projected into the far-field. It should be noted that, at specific wavelengths, for example, at 550 nm (for both the systems), the system has maximum intensity towards only one direction in the ϕ plane and it is not axially symmetric. For not all wavelengths, it holds true. Essentially, for all the investigated cases, having an excitation wavelength at the blue-side of the spectrum results in interesting emission scenarios.
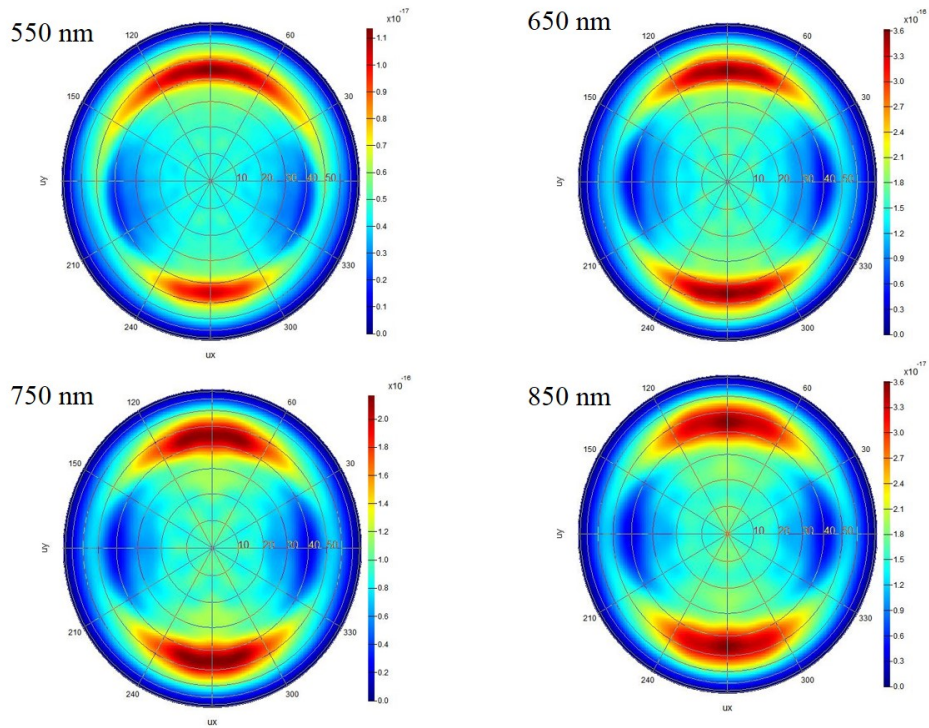

Figure 3.18: *Far-field radiation patterns for 90° angled gold nanorod dimers with 3 nm gap size at (a) 550 nm (b) 650 nm (c) 750 nm and (d) 850 nm. At 550 nm, the forward-to-backward intensity ratio is more compared to the other regions.*
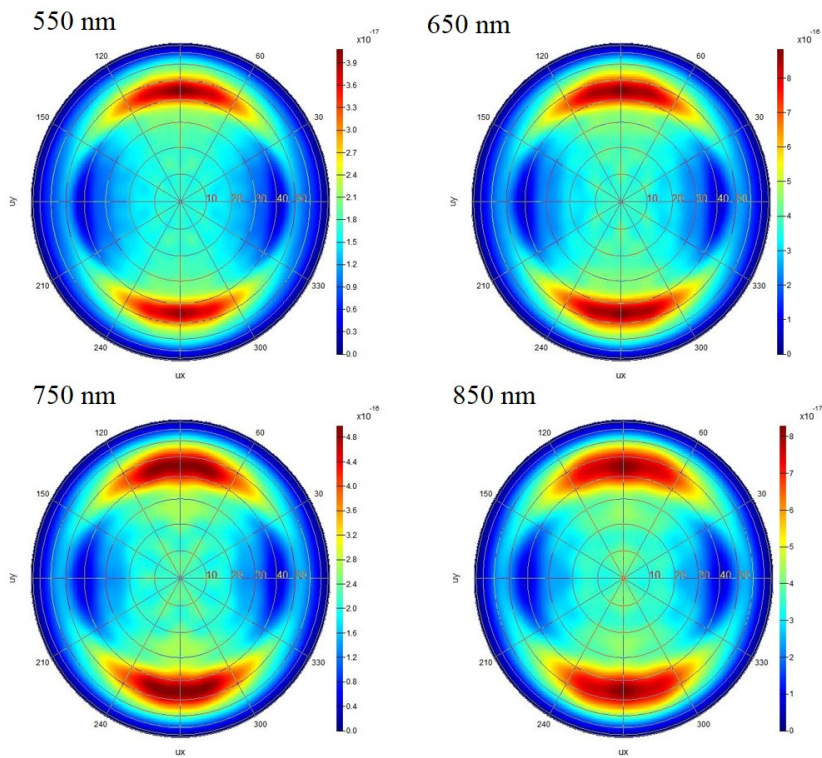
Figure 3.19: *Far-field radiation patterns for 135° angled nanorod dimers with 3 nm gap size at (a) 550 nm (b) 650 nm (c) 750 nm and (d) 850 nm*

Such an observation demands further investigation for complete understanding. Nevertheless, it points out that gold nanorod dimers of asymmetric orientations are promising candidates for optical antenna applications.

Chapter 4

Summary and Future directions

In this work, gold nanorods of an average aspect ratio of 3 were synthesized by a bottom-up method which resulted in single crystalline nanostructures and they were characterized using different experimental techniques. Inorder to get insight into the near-field and far-field properties, electrodynamic simulations were performed. Comparison of scattering spectra of single nanorods in a homogeneous (in air) and inhomogeneous environment (on a glass substrate) were done. How the gap size influences the scattering spectra of end-to-end connected and side-by-side aligned dimers was addressed. Studies on dimers of different inter-rod angles and excitation polarizations unravelled important information about their viability as nanoscale optical antennas. It was found that, the inter-rod angle and the excitation wavelength play a critical role in determining far-field properties. For particular angled dimers, the scattering spectrum showed an asymmetric Fano-like line profile whose signature reflected in the directionality of far-field emission. At this Fano-like dip, the near-field pattern was also significantly different from the other two regions of the spectrum. Thus, it can be speculated that there is an intrinsic connection between the geometry of the nanostructure, Fano-like resonance and the directionality of far-field emission.

We further plan to come up with a model to explain the three-way connection we concluded from our observations. We also plan to incorporate emitters (like molecules) in the gap between these nanorods and intend to study field enhancement factors as well as directionality of emission with an aim to model angled gold nanorod dimers with particular gap sizes as efficient Raman optical antennas. In that context, the three wavelength regions explored in this work would correspond to the anti-Stokes, Rayleigh and Stokes regions in the case of Raman spectra. Since the Fano-dip for specific angles occurred at the blue-side of the spectrum, it is at the anti-Stokes region. The

anomalous near- and far-field properties observed at this region paves way to explore how the geometry of gold nanorod dimers affect near-field Raman enhancement factors as well as the radiation patterns.

Bibliography

1 Hecht, E. G. A. R. Optics. (Addison-Wesley, 2002)

2 Maier, S. A. Plasmonics: Fundamentals and Applications (Springer, 2007)

3 Pelton M, Bryant G, Introduction to metal nanoparticle plasmonics (Wiley, 2013)

4 Jackson, J. D. Classical electrodynamics (Wiley, 1975)

5 G. Mie, Ann. Phys. 1908, 330, 377

6 R. Gans, Ann. Phys. 1912, 342, 881

7 J. Wang, Chem. Soc. Rev., 2013, 42, 2679

8 K. Miyano, Appl. Phys. Lett. 2003, 83, 4625

9 P. Mulvaney, J.Appl.Phys. 2006, 99, 123504

10 M. Staffaroni, Photonics and Nanostructures Fundamentals and Applications, 2012, 10, 166

11 Y. Zhu, Opt. Exp., 2009,17, 6407

12 P. Nordlander, Science, 2003, 302, 411

13 N J. Halas, Acc. Chem. Res., 2007, 40, 53

14 G. Haran Volume 2014, 21, 26

15 P. Mulvaney, Nano let., 2009, 9, 1651

16 P. Nordlander, Nat. Mat., 2010, 9, 707

17 Stutzman, W. L. T. G. A. Antenna theory and design. (Wiley, 1981)

18 Lee, B, Sensors 2011, 11, 10907

19 J Wessel, J. Opt. Soc. Am. B, 1985, 2, 1538

20 L Novotny, J. Adv. Opt. Photon., 2009, 1, 438

21 van Hulst, Nat. Phot., 2011, 5, 83

22 V Giannini, Chem. rev.2011, 111, 3888

23 B Hecht Rep. Prog. Phys., 2012, 75, 024402

24 H Acar, ACS Nano, 2012, 6, 8226

25 van Hulst, Nature, 2007, 448, 141

26 L Novotny, Nature, 2008, 455, 887

27 A G Curto, Science, 2010,329, 930

28 C J F Bottcher, Theory of Electric Polarisation (Elsevier, 1973)

29 D Roylance, Finite Element Analysis. 2001

30 J Parsons,Jour. of Mod. Opt., 2010, 57, 356

31 D David and W Challener, Modern introduction to surface plasmons
   Theory, modelling and applications (Cambridge, 2010)

32 M. A. El-sayed, Chem. Mater. 2003, 15, 1962

33 P. Mulvaney, Phy. Chm. Chm. Phy., 2013, 15, 4258

34 K G Thomas, J. Phy. chm. Lett., 2011, 2, 610

35 K G Thomas, Adv.Mater., 2008, 20, 4300

36 A P Alivisatos, J. Phy. Chm., 1996,100, 13226

37 C J Murphy, Phy. Chm B., 2001, 105, 4065

38 J C Mitchell, Langmuir, 1998, 14, 4724

39 N Fang, ACS Nano, 2010,12, 7667

40 J Wang, ACS Nano, 2008, 2, 677

41 J Murphy, J. Phys. Chem. Lett. 2010, 1, 2867

42 M Orrit, Nano Lett. 2014, 14, 915

43 K J Thomas, Nanoscale, 2014, 6, 10454

44 M P Pimeni, J. Phys. Chem. B, 2005, 109, 13138

45 N G Khlebtsov, J. Phys. Chem. C 2007, 111, 11516

46 J Wang, Nano Lett.2008, 2, 677

47 R. W. Christy, Phys. Rev. B 1972, 6, 4370

48 E. D. Palik, Handbook of Optical Constants of Solids (Elsevier Science, 2012)

49 M Orrit, ACS Nano. 2014, 8, 4440

Appendix A

Far-field properties in FDTD

Though FDTD is a near-field calculation, it is possible to compute far-field properties from near-field properties. Consider an incident field with a sinusoidal time dependence. The phase and the maximum value of amplitude should be determined in the beginning, so that these values can be determined as a function of time. Suppose the instantaneous amplitudes of the fields were calculated at two different times separated by a period of $\pi/2$. This gives the information about the peak value of amplitude and phase of the scattered field. At a given point of time t_1, let F_1 be the value of the computed field

$$F_1 = E_1 \sin(\omega t_1 + \phi) \tag{A.1}$$

At time t_2, which is a quarter perid after F_2,

$$F_2 = E_1 \sin(\omega t_1 + \phi + \pi/2) \tag{A.2}$$

The total fiel amplitude is given by,

$$\sqrt{(F_1)^2 + (F_2)^2} = \sqrt{(E_1 \sin(\omega t_1 + \phi))^2 + (E_1 \sin(\omega t_1 + \phi + \pi/2))^2} \tag{A.3}$$

$$= \sqrt{(E_1 \sin(\omega t_1 + \phi))^2 + (E_1 \cos(\omega t_1 + \phi)^2} \tag{A.4}$$

The phase ϕ is,

$$\phi = \tan^{-1}\left(\frac{F_1}{F_2}\right) \tag{A.5}$$

The phase ϕ is,

$$= \tan^{-1}\frac{E_1 \sin(\omega t_1 + \phi)}{E_1 \sin(\omega t_1 + \phi)} \tag{A.6}$$

43

Scattering coefficient can be computed by considering a closed box around the object that scatters light. The phase and amplitude of electric and magnetic fields on all the surfaces of the box can be obtained from (A.5) and (A.6). Integrating the Poynting vector over the surface of the box gives the total power. If $S_x(i_1, j, k)$ is the outward normal component of the Poynting vector at a cell defined by (i_1, j, k) on the face of the box at $x = i_1$ and $S_x(i_2, j, k)$ is the outward normal component of the Poynting vector at a cell defined by (i_2, j, k) on the face of the box at $x = i_2$, and $\Delta A_x = \delta y . \delta z$ is the surface area of each cell on the above two faces, the total power power flowing out of the box is,

$$P_{scat} = \sum_{j,k} [S_x(i_1, j, k) + S_x(i_2, j, k)] \Delta A_x$$

$$+ \sum_{i,k} [S_y(i, j_1, k) + S_x(i, j_2, k)] \Delta A_y$$

$$+ \sum_{i,j} [S_z(i, j, k_1) + S_z(i, j, k_2)] \Delta A_z$$

The incident wave has power per unit area as,

$$S_{inc} = \frac{1}{2\eta} \tag{A.7}$$

where, the impedance η is

$$\eta = \sqrt{\mu/\epsilon} \tag{A.8}$$

The scattering cross-section is,

$$C_{scat} = \frac{P_{scat}}{S_{inc}} \tag{A.9}$$

which comes out to be,

$$C_{scat} = (2\eta) \sum_{j,k} [S_x(i_1, j, k) + S_x(i_2, j, k)] \Delta A_x$$

$$+ \sum_{i,k} [S_y(i, j_1, k) + S_x(i, j_2, k)] \Delta A_y$$

$$+ \sum_{i,j} [S_z(i, j, k_1) + S_z(i, j, k_2)] \Delta A_z$$

Absorption cross section can also be obtained in a similar manner.